Publishing House
AKAPIT

COMPUTER METHODS IN MATERIALS SCIENCE

Informatyka w Technologii Materiałów

Vol. 10, 2010, No. 2

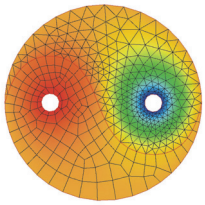

NUMERICAL ANALYSIS OF THE DESIGN AND RESEARCH INTO THE PRODUCTION OF SHELL MADE OF MAGNESIUM ALLOY

SEMAR BASYUK[1], PAVEL PETROV[2,*], VICTOR VORONKOV[2], ALEXEJ PLOTNIKOV[2], MAXIM SHAJXULOV[3]

[1] Disk BS Ltd., Russia
[2] Moscow State Technical University "MAMI", B.Semenovskay str. 38, 107023 Moscow, Russia
[3] Joint-Stock Company "SMK", Russia
**Corresponding Author: petrov_p@mail.ru (P. Petrov)*

Abstract

The paper describes the unified approach to the development of the design of the magnesium automotive wheels. It focuses on two subjects: the effect of the wheel geometry on its strength and the effect of the forging die geometry on the loading conditions during the hot forging of the preform of the wheel. The investigation within the scope of the paper has been done on the basis of the finite-element (FE) modelling. It was carried out by means of the FE commercial codes T-FLEX Analysis and QFORM-2D.

The modelling of the strength of the wheel results in the comparative analysis of the wheels with different geometries in terms of the safety factor by equivalent stress. The FE modelling of the hot forging of the preform of the wheel shows capabilities of the chosen scheme of the combined extrusion-type forging. The relationships between the geometrical parameters of the die and the technological parameters of the forging were established on the basis of numerical simulation.

Key words: magnesium alloy, automotive wheel, wheel strength, extrusion-type forging, thin-walled shell, numerical simulation, finite-element method, FEM, safety factor

1. INTRODUCTION

The review of the design of modern automotive light-weighted wheels allows to evolve 3 groups of the wheels (Basyuk, 2009). The classification in (Basyuk, 2009) is based on the technological aspect and it implies that a wheel is manufactured from a workpiece formed by the hot forging. Figure 1 shows the typical geometry of the wheels within each of the marked groups.

The typical workpiece for wheels related to the group 1 is a cup-type workpiece with one flange at its end and with the tube extension at its bottom part. The group 2 contains the wheels produced from a workpiece with two-sided flanges and with the tube extension at its bottom part. The group 3 relates to a cup-shaped workpiece with two-sided flanges and with the centre boss shifted inside the wheel hub.

Generally, an automotive wheel represents an axisymmetrical space shell either conical or cylindrical with the non-constant cross-section in the longitudinal direction (see figure 1). To choose a technological scheme of forging for the production of the workpiece of the wheel, several parameters should be taken into consideration, i.e. shape and quality of the workpiece, its strength as well as operational characteristics, the time of preproduction and the cost of the forged wheel.

ISSN 1641-8581

The objectives of the present paper are: (i) to investigate the effect of the geometry of a magnesium wheel on its strength in terms of the safety factor measured by the equivalent stress; (ii) to investigate the effect of the geometry of dies for forging of a preform of the magnesium wheel on the loading conditions during forging at elevated temperature. It is considered that the material of the wheel is magnesium alloy MA2-1. This alloy is produced in accordance with the Russian standard and it is similar to *AZ31* alloy.

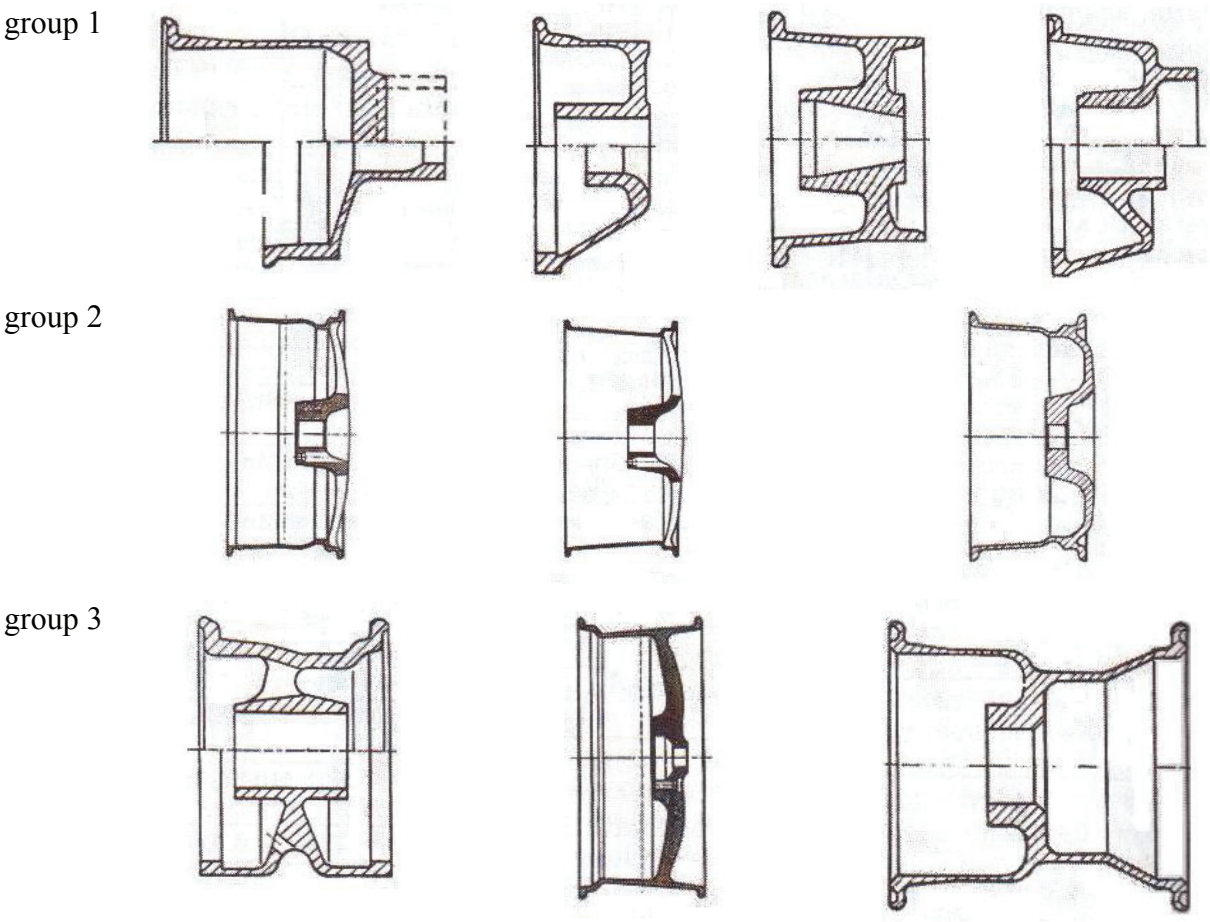

Fig. 1. *Types of the automotive wheels (Basyuk, 2009).*

2. NUMERICAL SIMULATION OF THE WHEEL STRENGTH

Strength characteristics of the wheel can be estimated by means of standardized tests. For instance, in Russia these tests are carried out in accordance with the *GOST* 50511 standard. The fatigue test under simultaneous application of the bending as well as torque to the tested wheel, is one of the common testing methods. This test allows to investigate the effect of the side forces on the wheel when the car moves along the road turn. According to the scheme of this test, the wheel is clamped on the flat surface and the bending moment is applied to it (figure 2). This moment is created with the help of the lever connected to the centre boss of the wheel (see figure 2). The torque is also applied to the wheel and it is transferred through the axis which supports the wheel.

In the present paper the numerical simulation of the test mentioned above was carried out. Different geometries of the wheel were investigated (figure 3). In reality, the test is performed under dynamic loading conditions while the numerical simulation corresponds to the fixed value of the turning angle. Because of that the torque moment is not shown in figure 2(a). The value of the turning angle was equal to zero.

The maximum value of the bending moment is estimated by the formula:

$$M_{\max} = KF_v(\mu R + d), \tag{1}$$

where K = overload factor, assumed to be 2.0; F_v – maximum static vertical force applied to the wheel; μ – traction coefficient between the tyre and the road coating, assumed to be 0.9; R – static radius of the

tyre of the maximum size; d – rim offset (see figure 2).

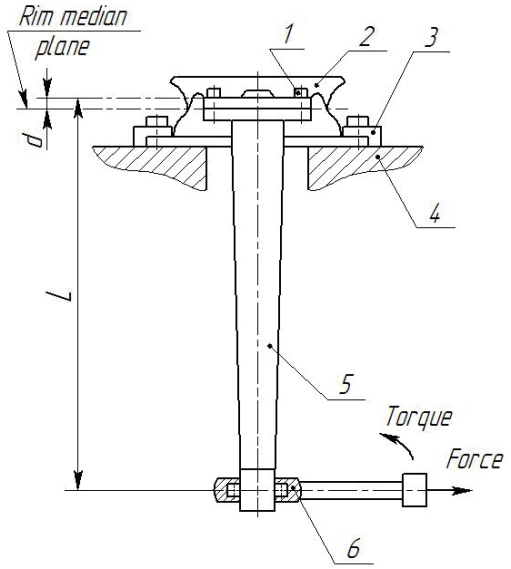

a) scheme of the standardized test (Baturin, 2006): 1 – wheel transfer means; 2 – wheel; 3 – rim fastener; 4 – support plate; 5 – lever; 6 – bearing

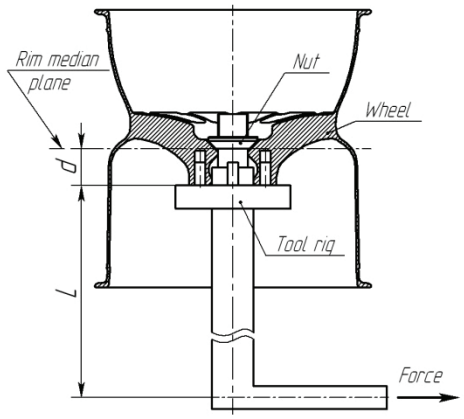

b) scheme of the FE-simulation

Fig. 2. *Scheme of the test.*

According to the technique of the test, the maximum value of the bending moment should be equal to 3.46 MN×mm. This value was calculated with assumptions that the maximum value of the static load applied to the wheel, F_v, is 5 kN, the static radius, R, is 330 mm and the rim offset, d, is 49 mm. Mechanical and physical properties of the Mg-alloy as well as its chemical composition, are given in table 1-3 correspondingly. Numerical simulation of the standardized test (see figure 2) was carried out by means of finite-element (FE) system T-FLEX Analysis (Top Systems Ltd., Russia).

The investigated wheel is represented by a space shell supported with load-bearing elements (rims, stiffening ribs, centre boss etc.). The total volume of the wheel is conditionally divided into 5 elementary volumes. Each elementary volume corresponds to either a shell part of the wheel or to a load-bearing element (figure 4).

Table 1. *Mechanical properties of the MA2-1 alloy.*

Elastic modulus, 10^4 MPa	Yield strength $\sigma_{0,2}$, MPa	Ultimate strength σ_B, MPa	Elongation, δ, %
4.2	160	265	12

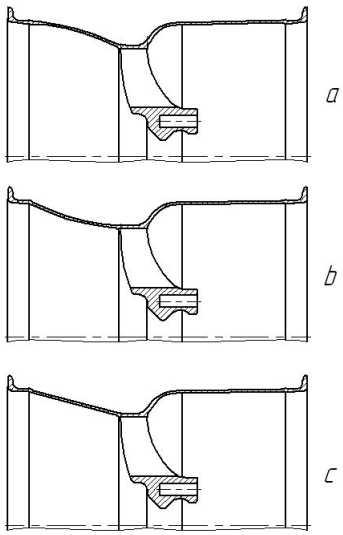

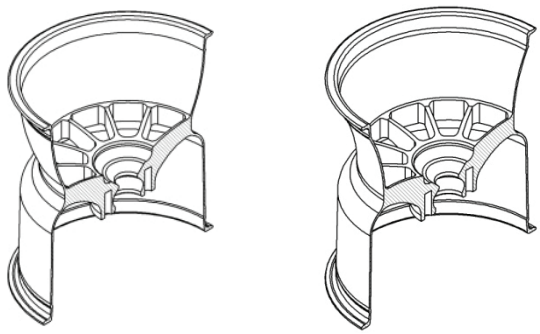

type a – conical shell with positive curvature of its surface

type b – conical shell with negative curvature of its surface

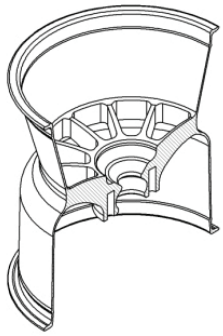

type c – conical shell with neutral curvature of its surface

Fig. 3. *Geometry of the wheel in longitudinal section (Basyuk, 2009).*

Table 2. *Physical properties of the MA2-1.*

Density, kg/m^3	Linear expansion coefficient at 20-100°C, $\alpha\times10^6$, 1/°C	Thermal conductivity, W/(m·K)	Specific heat capacity, kJ/(kg·K)	Specific resistance, $r\times10^9$, Ω·m
1790	26	83.8	1.05	120

Table 3. *Chemical composition of the MA2-1 alloy (GOST 14957-76; appr. AZ31).*

Element	Mg	Al	Mn	Zn	Si	Fe	Ni	Cu	Be	Ca
%	base	3.8-5	0.2-0.6	0.6-1.5	0.15	0.05	0.005	0.05	0.02	0.1

Table 4. *Distribution of the volumes between the characteristic elements of the wheel.*

Type of wheel	Total volume, mm^3	V_1, %	V_2, %	V_3, %	V_4, %	V_5, %
a	2211050	7.56	15.11	17.37	52.10	7.86
b	2192406	7.63	14.39	17.52	52.55	7.93
c	2197619	7.61	14.59	17.47	52.42	7.91

The major difference between the investigated geometries of the wheel is the curvature of the conical shell between the front rim and centre boss (see figure 3). It results in the different values of the volume V_2 (table 4). Depending on the type of the wheel, the volume of the load-bearing elements changes from 66.91 % to 67.21 % of the total volume of the wheel. At the same time, the total volume of the shells, which the wheel includes, changes from 32.99 % to 33.07 % of the total volume of the wheel (see table 4).

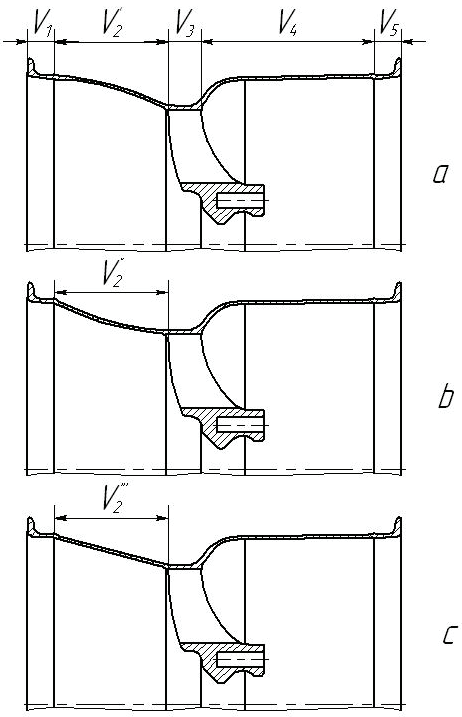

Fig. 4. *Scheme for the definition of the elementary volumes in the wheel:*
V_1 – volume corresponding to the front rim (flange);
V_2 – volume corresponding to the shell between the front rim and the centre boss;
V_3 – volume corresponded to the centre boss;
V_4 – volume corresponding to the shell between the centre boss and the back rim (flange);
V_5 – volume corresponding to the back rim.

3. NUMERICAL SIMULATION OF THE TECHNOLOGY OF FORGING

The workpiece for the investigated geometries of the wheel can be obtained by hot forging. One of the possible schemes of hot forging was investigated in the present work. This scheme implies the extrusion of the material in both radial and backward directions. To perform numerical investigation of this process, the die-set for the combined extrusion-type forging was designed (figure 5). This die-set allows to analyze the material flow during the formation of the cylindrical shell of the wheel (see figure 3). The numerical simulation of the material flow was carried out by means of the finite-element (FE) system QFORM-2D (Quantor-Form Ltd., Russia). This commercial FE-system suits well for numerical modelling of the technologies of open die and close die forging, as well as rolling.

4. RESULTS

4.1. Effect of the geometry of the wheel on the safety factor

Numerical simulation of the standardized test (see figure 2) resulted in the data which illustrates the effect of the curvature of the conical shell on the strength of the wheel. The strength of the wheel was estimated by the safety factor.

The value of the safety factor can be established by the following formula:

$$K = \frac{[\sigma]}{\sigma_i}, \qquad (2)$$

where K = safety factor by equivalent stress; σ_i – equivalent stress taking into account the stress tensor components

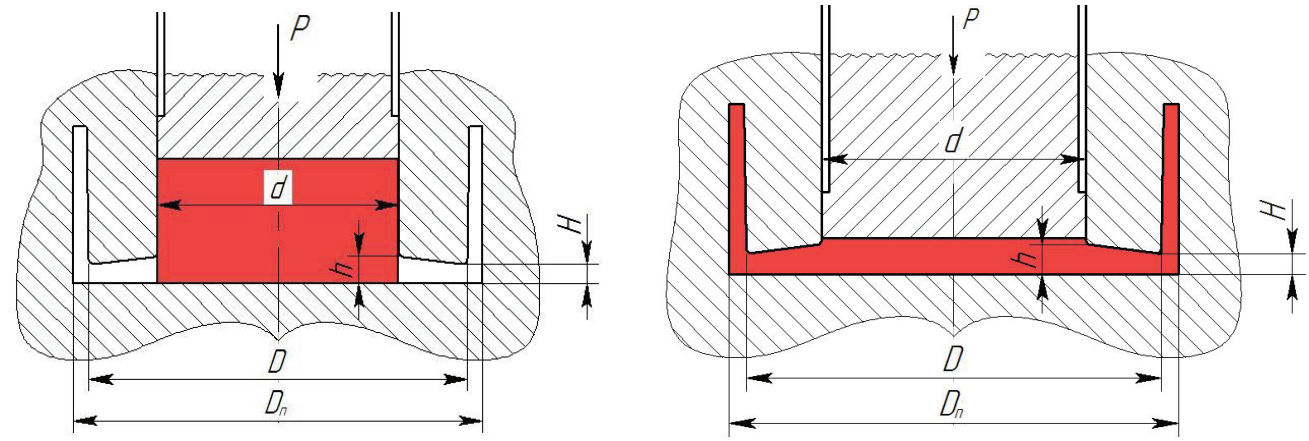

a) drawing of the die set

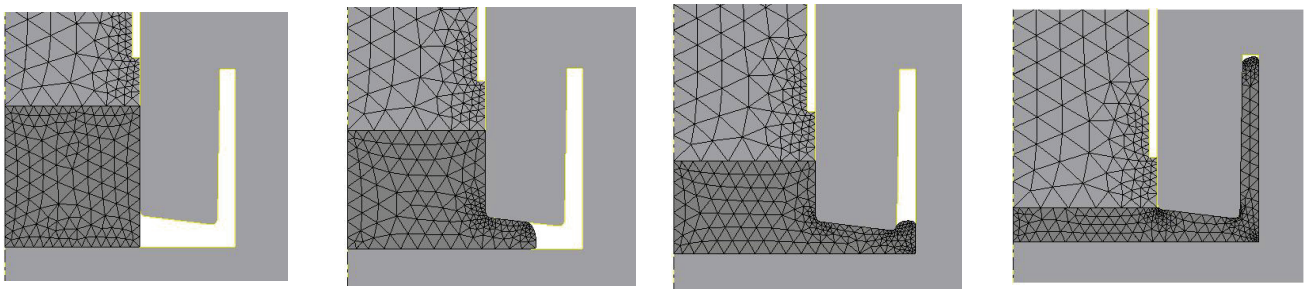

initial position of upper die and workpiece | first stage in progress | beginning of the second stage | end of the second stage

b) FE model of the process

Fig. 5. *Scheme of the hot forging of cylindrical shell.*

$$\sigma_i = \frac{1}{\sqrt{2}}\sqrt{(\sigma_x - \sigma_y)^2 + (\sigma_y - \sigma_z)^2 + (\sigma_z - \sigma_x)^2 + 6(\tau_{xy}^2 + \tau_{yz}^2 + \tau_{xz}^2)}, \quad (3)$$

$[\sigma]$ – the yield strength of the MA2-1 alloy (see Table 1).

Figure 6 shows the results of the FE simulation in terms of the safety factor. Several critical zones of the design of the investigated wheels are observed:

1) zone 1 is located at the middle of the wheel's spoke;
2) zone 2 corresponds to the area of the wheel, where two neighbour spokes connect to the centre boss of the wheel;
3) zone 3 corresponds to the area, where the spoke connects to the front rim of the wheel.

Change in the curvature of the conical shell (see figure 6) leads to increase of the value of the safety factor within the critical zones. It is assumed that the wheel of type «a» is the reference wheel. The comparisons between the wheels of type «c» and «a» as well as between the wheels of type «b» and «a» were performed in terms of the safety factor.

For the wheel of type «c» the safety factor in zone 1 is about 17% higher than the corresponding value computed by numerical simulation in the same zone of the wheel of type «a». The change in the curvature of the shell results in the increase in the safety factor of about 11% for the wheel of type «c» in zone 2. In zone 3 the slight decrease in the safety factor for the wheel of type «c» is observed. Here the safety factor reaches the value of 1.917 for the wheel of type «c», while for the reference wheel it is equal to 2.074.

For the wheel of type «b» the safety factor in zone 1 is about 1% higher, while in zone 2 and 3 it is about 6.4% and 11.6% lower, respectively, than the corresponding values computed by numerical simulation in the same zones of the wheel of type «a».

4.2. Effect of the geometry of the forging dies

The analysis of the results of the experimental tests (Petrov et al., 2010) shows that the die filling occurs due to the material extrusion in both the radial and the backward directions. Considering that, the material flow is divided into the following two stages:

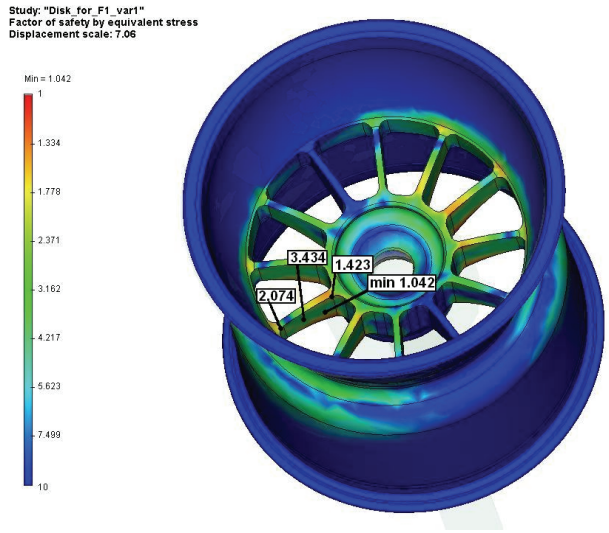

type a – conical shell with positive curvature of its surface

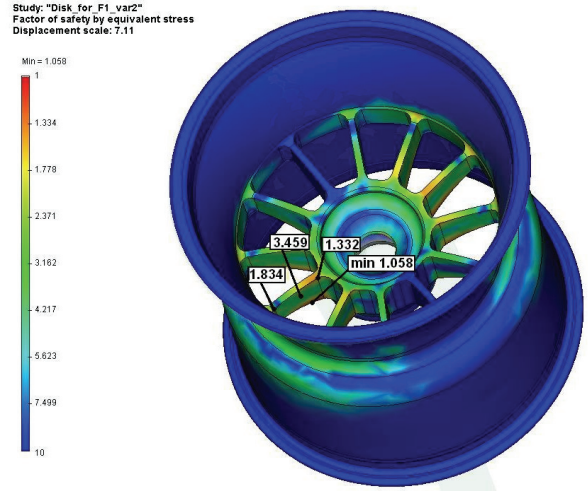

type b – conical shell with negative curvature of its surface

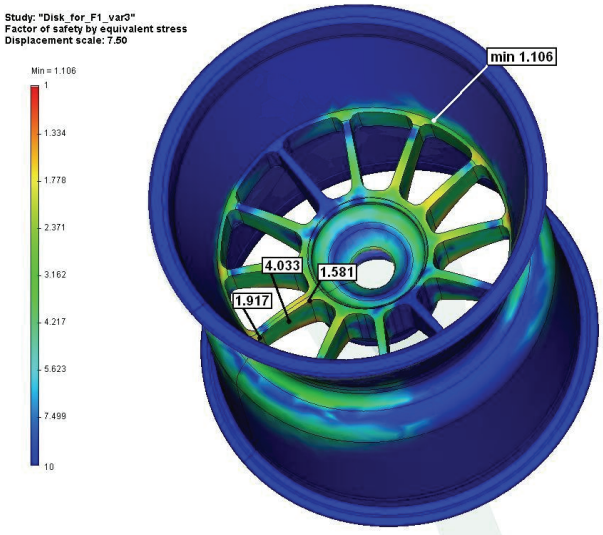

type c – conical shell with neutral curvature of its surface (minimum value of the safety factor corresponds to the inner surface of the spoke)

Fig. 6. *Distribution of the safety factor based on the equivalent stress.*

1) First stage – *extrusion in the radial direction* (see figure 5b) – starts from the first contact between the upper die (punch) and the workpiece and lasts till the complete filling of the bottom cavity, which is formed between the clamping tool and the lower die. At the end of the first stage the extruded material contacts the wall of the container (see figure 5b).
2) Second stage – *extrusion in the backward direction* (see figure 5b) – starts after the contact of the deformed material with the container and lasts until the complete filling of the cavity, which is formed between the clamping tool and the container. For FE simulation by QFORM, the design of the die set was simplified. It is considered that the container and the clamping tool is as the one virtual tool. If in the experimental die set the clamping tool is fixed during the working stroke of the press, the mentioned simplification does not affect the accuracy of the results of the numerical simulation.

QFORM-2D code is based on the flow formulation where the independent variables are velocity vector and mean stress. In rigid-visco-plastic model the material is considered as incompressible, isotropic continuum and elastic deformations are neglected. The effective stress is a function of the effective strain, effective strain-rate and temperature. Friction model describing contact friction on the die surface proposed by Levanov (Levanov et al., 1976) is used in the QFORM-2D.

Numerical simulation by means of QFORM-2D was carried out considering that:

1) the flow stress-strain curves of the MA2-1 alloy is defined by isothermal flow curves determined on the basis of the results of the uniaxial compression tests performed under constant deformation conditions for different values of a strain rate as well as a temperature;
2) the isothermal flow stress-strain curves (figure 7) were derived from the load-displacement data as described by Petrov (2010);
3) the load-displacement data were obtained after the compression of the cylindrical specimens of the MA2-1 alloy at temperature of 390°C as well as 430°C and under constant strain rate of 0.001 s^{-1}, 0,01 s^{-1} and 0.4 s^{-1};
4) initial temperature of the workpiece is constant and equal to 400°C;
5) temperature of dies is constant and equal to 400°C during the deformation;

6) friction factor of a virtual lubricant is constant and equal to 0.22;
7) effective heat transfer coefficient of the lubricant is 1750 W/(m^2·K);
8) since the forging of the investigated shell is an axisymmetric process, the forming process is simulated for a half of workpiece (see figure 5);
9) a hydraulic press with die velocity of 2.0 mm/s is used for forging.

The effect of the die geometry was investigated numerically only. The variational parameters were the following (see figure 8): 1) draft angle α_1 of the end surface of the clamping tool; 2) draft angle α_2; 3) radius R_1; 4) radius R_2; 5) radius R_3; 6) height H defining the lowest point of the end surface of the clamping tool. The numerical values of these parameters are given in figure 8.

Figure 9 illustrates the typical force-time relationship of the investigated forging process. During the deformation, the loading path of a material point in the deforming zone is very complex, due to the change in the direction of strain (figure 9) (Petrov et al., 2010). Abrupt increase in the value of load corresponds to changing of a material flow direction due to the change in the die geometry. As the consequence, the material flows through the section A-A (figure 9) being extruded to the vertical cavity of the die due to backward extrusion. When the material points in the deforming zone flow through the section A-A, the transient change in the strain rate occurs. The value of strain rate $\dot{\varepsilon}$ increases over 10 times after the section A-A.

Material flow during the extrusion-type forging (see figure 5a) as well as the forming load depend on the temperature-strain rate conditions of the deformation, as well as on the die geometry. The ratio between the cross-section areas is the most important parameter of the investigated forging process. It has a great impact on the material flow. Here we investigate the effect of the areas S_d to S_D ratio, as well as the areas S_t to S_D ratio, on the forming force and strain rate history.

The parameter $S_d = \pi d h_d$ defines the area of the surface of the cylinder related to the diameter d and the height h_d (figure 10). The height h_d depends on the height H and on the angle α_1. The area $S_D = \pi D_H H_D$ is defined by the area of the surface of the cylinder related to the diameter D_H and the height of H_d (figure 10). The area $S_t = \pi t(t+D_t)$ is related to a conditional ring, which is formed due to the dissection of the vertical cavity by the horizontal plane at the height H_t (see figure 10). Parameters of S_d, S_D, S_t depend on the variational parameters given in figure 8.

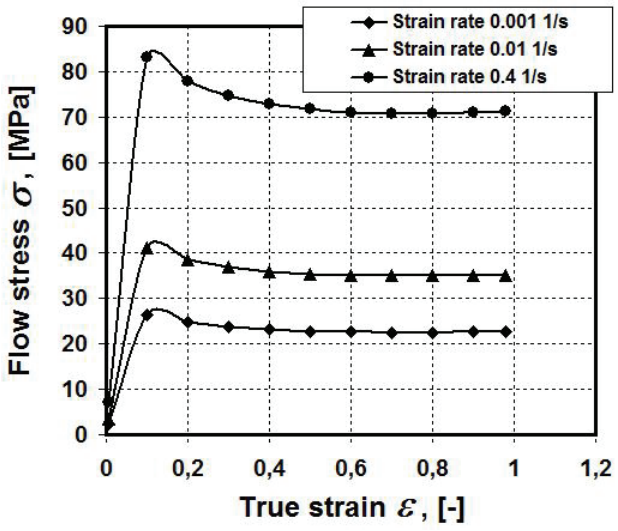

a) temperature of 390°C

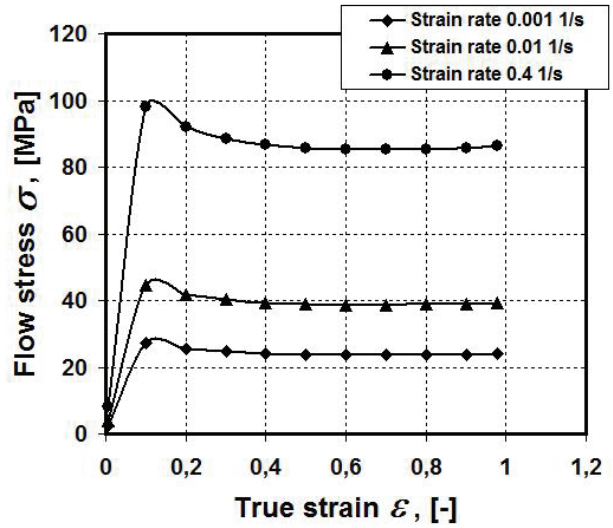

b) temperature of 430°C

Fig. 7. *Isothermal flow stress-strain curves of MA2-1 alloy.*

The effect of both ratios of S_d/S_D as well as S_t/S_D on forming load was investigated assuming that the force should be measured virtually at the beginning of the second stage of the investigated process, when the material flows through the radius R_2. As a result the material is extruded to the vertical cavity between the clamping tool and the container (see figures 8 and 9). To estimate the mentioned effect correctly, it is assumed that the angle α_2 does not influence the forming load at the beginning of the second stage of the forging process. The more material is extruded to the vertical cavity, the more the angle α_2 affects the value of the load.

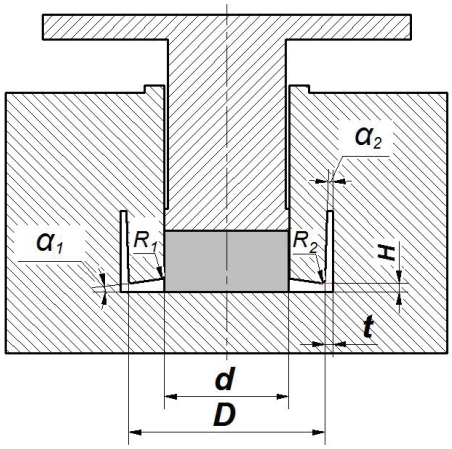

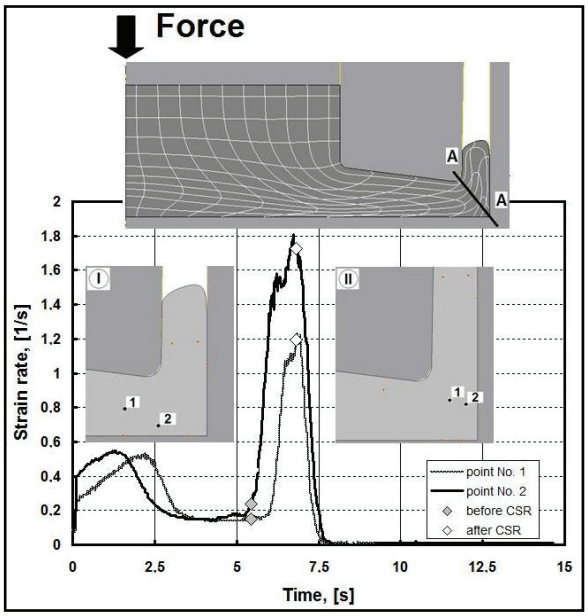

Fig. 9. *Typical strain-rate history: CSR – change in strain rate*

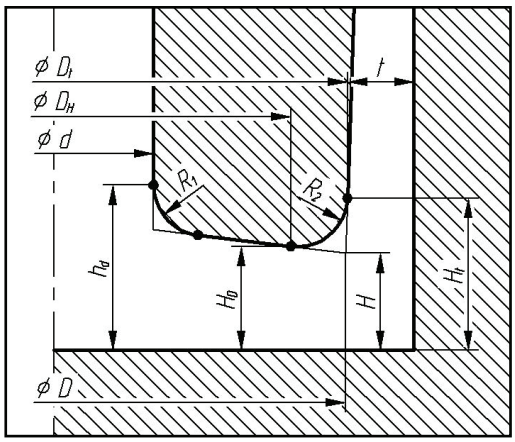

Fig. 10. *Scheme for the definition of the cross-section areas.*

Figure 11 shows the dependence between the forming load and the both ratios S_d/S_D and S_t/S_D. Squared dark points correspond to the FE modelling of the process. Each of these points refers to one numerical computation by means of QFORM-2D

Parameter	Value
Angle α_1 α_2	7°; 10° 1°; 2°; 3°; 4°; 5°
Radius R_1 R_2	1; 3; 5 1; 3; 5
Height H	2; 3,5; 5; 7; 10; 15

Fig. 8. *Scheme for FE simulation of the forging process.*

code. Each of the FE simulations was carried out for fixed set of the variational parameters (α_1, R_1, R_2, H) (table 5).

Table 5. *Set of the variational parameters for FE modelling.*

Radius R_1 and R_2, mm	Height H, mm					
	2	3,5	5	7	10	15
1	The draft angle α_1 is equal to either 7° or 10°					
3						
5						

Figure 12 illustrates the typical force-time relationship, which characterizes the forging process. It is observed that the plots have similar shape. Peculiarity of the investigated process is linked to the abrupt increase in the forming load. This increase happens between the 5th and 6th seconds of the deformation (see figure 12). The increase in the forming load is due to the abrupt increase in the strain rate, which occurs when the deformed material flows through the radius R_2 and further is extruded into the vertical cavity (see figure 9).

Depending on the values of the parameters α_1, R_1, R_2 and H, the slope of the plot corresponds to the abrupt increase in strain rate changes. It occurs either earlier than in 5th seconds after the beginning of the forging process or later. Increasing in the value of the radii R_1 and R_2 causes the increase in the value of the areas S_d and S_D. The consequence of that is decreasing the forming load during the transient change in the strain rate (see figure 12). From the theoretical point of view, knowing the effect of the ratio S_t/S_D on the value of the strain rate of a material point which flows through the section *A-A* (see figure 9), as well as on the change in the strain rate $\Delta\dot{\varepsilon}$ during the transient process, is of a great interest.

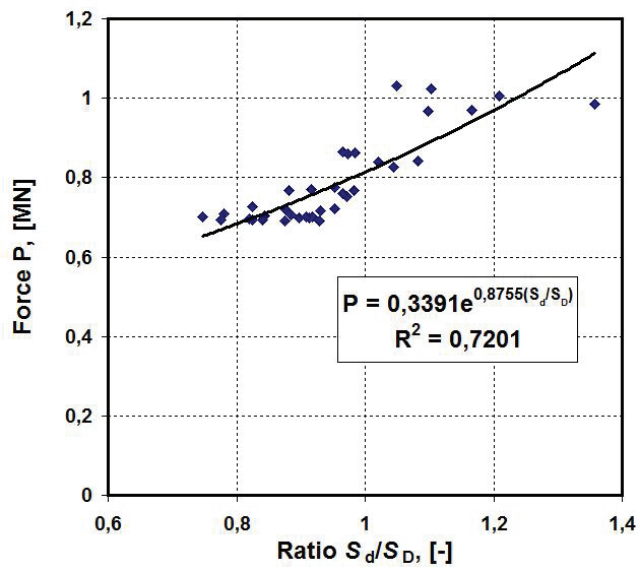

a) angle $\alpha_2 = 1°$

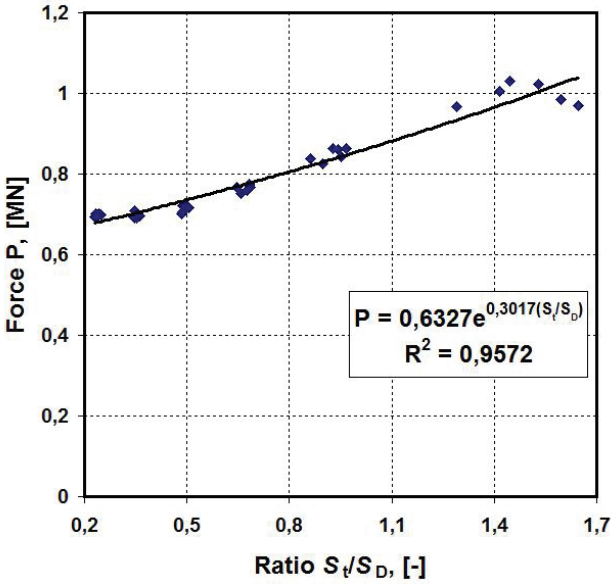

b) angle $\alpha_2 = 1°$

Fig. 11. *Plot of the force versus ratio of cross-section area.*

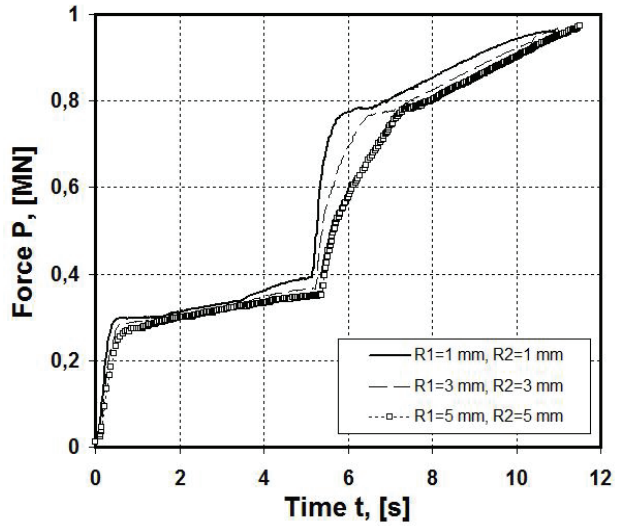

Fig. 12. *Plot of the force versus time of the forming process ($\alpha_1 = 7°$, $\alpha_2 = 1°$, $H = 5$ mm).*

The change in strain rate is calculated from the formula:

$$\Delta\dot{\varepsilon} = \dot{\varepsilon}_{csr} \Big/ \dot{\varepsilon}_{before}\,, \tag{4}$$

where $\dot{\varepsilon}_{crs}$ – strain rate of a material point, which flows through the section *A-A*; $\dot{\varepsilon}_{before}$ – strain rate of the material point before its flow through the section *A-A*.

To investigate mentioned effects numerically it is assumed that the height H is the only one variational parameter and it has the values given in figure 8. The other parameters (α_1, α_2, R_1, R_2) are fixed and equal to 1 mm, 1 mm, 7° and 1°, respectively. The material points taken into account for this computation are located at the equidistance from the radius R_2.

Figures 13-15 show the results, which illustrate the effect of the ratio S_t/S_D on the strain rate, as well as on the $\Delta\dot{\varepsilon}$. Despite the increase in the strain rates $\dot{\varepsilon}_{src}$ and $\dot{\varepsilon}_{before}$, the change in strain rate $\Delta\dot{\varepsilon}$ decreases with the increase in the ratio S_t/S_D (figure 15). The variation of $\Delta\dot{\varepsilon}$ with the ratio S_t/S_D is found to fit well the logarithmic function (see figure 15), while the strain rate-ratio relationships are fitted with exponential functions (see figure 13 and figure 14). When the ratio S_t/S_D becomes equal to 1 or more, the value of $\Delta\dot{\varepsilon}$ does not change significantly.

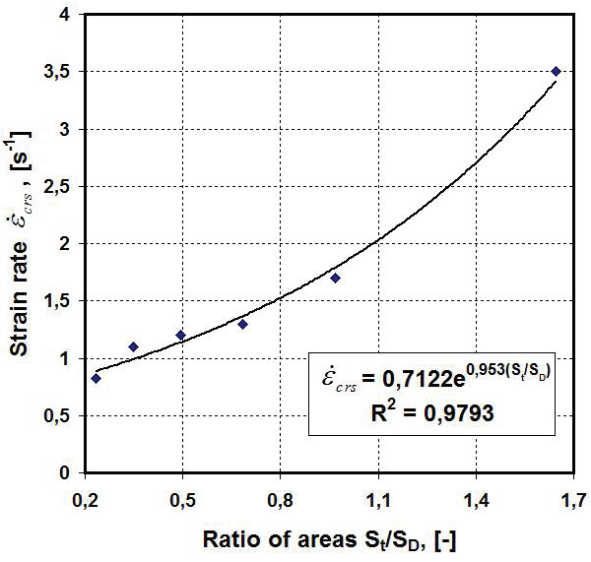

Fig. 13. *Plot of strain rate $\dot{\varepsilon}_{crs}$ versus S_t/S_D.*

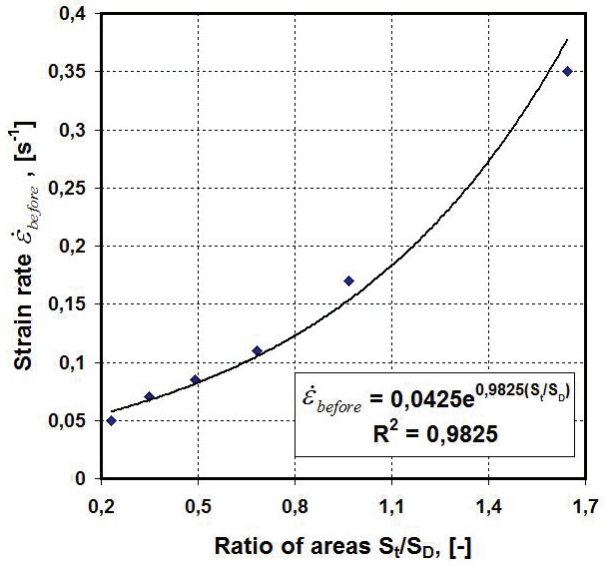

Fig. 14. Plot of strain rate $\dot{\varepsilon}_{before}$ versus S_t/S_D.

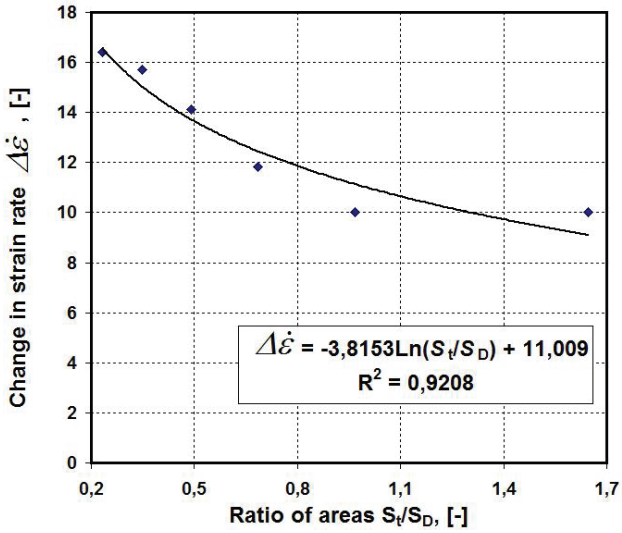

Fig. 15. Plot of change in strain rate $\Delta\dot{\varepsilon}$ versus S_t/S_D.

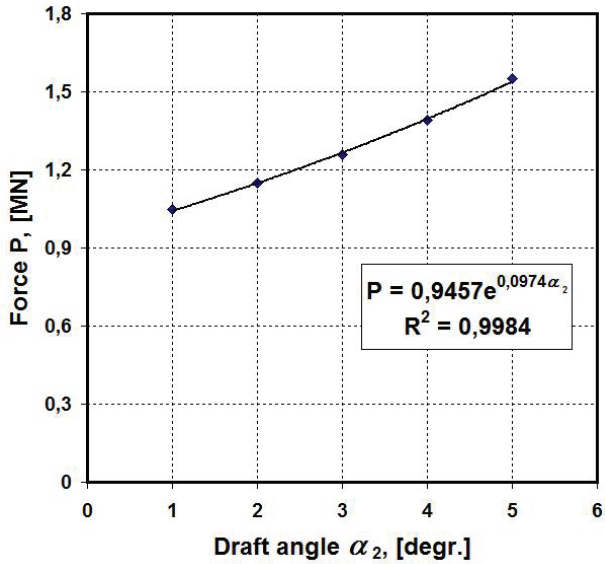

Fig. 16. Plot of force versus angle α_2.

During the second stage of the investigated forging process, the forming force depends on the draft angle α_2. The value of the angle α_2 defines the geometry of the vertical cavity, which is formed between the clamping tool and the container (see figure 8). During the deformation the angle α_2 is constant. The increase in the angle α_2 implies the change in the geometry of the clamping tool. The force-angle relationship can be fitted well with the exponential function (see figure 16). The positive effect of the reduction of the angle α_2 is connected with the less material loss for machining of the forged part.

5. CONCLUSIONS

This paper presents the method of the selection of the geometry of the magnesium wheel on the basis of the numerical simulation of its strength and the technology of hot forging. It is shown that the change in the curvature of the shell, which the wheel consists of, has the significant effect on the strength of the wheel in terms of the safety factor based on the equivalent stress. On the other hand, the ratios S_d/S_D and S_t/S_D are the major parameters, which allow to control the material flow during the extrusion type forging according to the scheme «radial extrusion»-«backward extrusion». This scheme was investigated in the paper.

The analysis presented here can be extended to include more complex material flow during the hot forging of shell-shaped parts. This can be relevant for the numerical simulation of the combined extrusion-type forging in accordance with the scheme «radial extrusion»-«simultaneous backward and forward extrusion». This scheme has more potentialities in comparison with the investigated scheme of forging.

REFERENCES

Basyuk, S.T., 2009, *Bulk forging of light alloys with hydraulic presses*. Second edition. Sport&Culture-2000, Moscow.

Baturin, A.I., 2006, Stress-strain state of the automotive wheels, *Forging and stamping production, Metal forming*, 7, 26-31.

Basyuk, S.T., 2009, *Forged wheel discs in light alloys for sport cars*. Sport&Culture-2000, Moscow.

Petrov, P.A., Gnevashev, D.A., Voronkov, V.I., Grinberg, I.V., 2010, Physical and mathematical modelling of the technology of thin-walled shells extrusion-type forging, *Technology of Light Alloys*, 2, (in print).

Petrov, P.A., 2010, Determination of the «isothermal» flow stress-strain curve of aluminium alloy of V95, *Material Working by Pressure*, Kramatorsk, Ukraine, (in print).

Levanov, A.N., Kolmogorov, V.L., Burkin, S.P., Kartak, B.R., Ashpur, U.V., Spasskiy, U.I., 1976, *Contact Friction in Metal Forging*, Metallurgia, Moscow.

NUMERYCZNA ANALIZA PROJEKTOWANIA ORAZ BADANIA NAD WYTWARZANIEM KÓŁ ZE STOPÓW MAGNEZU

Streszczenie

W artykule opisano zunifikowane podejście do projektowania felg samochodowych ze stopów magnezu. Rozważono dwa aspekty: wpływ kształtu felgi na jej parametry wytrzymałościowe oraz wpływ kształtu kowadeł na siły w procesie kucia. Badania przeprowadzono w oparciu o symulacje metodą elementów skończonych (MES) z wykorzystaniem komercyjnych programów T-FLEX Analysis oraz QFORM-2D.

W wyniku modelowania wytrzymałości felgi uzyskano porównanie różnych kształtów felg w aspekcie ich bezpieczeństwa, przyjmując za kryterium stan naprężenia. Symulacje MES procesów plastycznego kształtowania felg wykazały korzystne cechy wybranych połączonych schematów wyciskania i kucia. Na podstawie numerycznych symulacji wyznaczono zależności pomiędzy parametrami geometrycznymi kowadeł i parametrami technologicznymi procesu.

Received: May 2, 2010
Received in a revised form: May 18, 2010
Accepted: May 19. 2010